We are IntechOpen, the world's leading publisher of Open Access books
Built by scientists, for scientists

4,800
Open access books available

122,000
International authors and editors

135M
Downloads

Our authors are among the

154
Countries delivered to

TOP 1%
most cited scientists

12.2%
Contributors from top 500 universities

CLARIVATE ANALYTICS
BOOK CITATION INDEX
INDEXED

WEB OF SCIENCE™

Selection of our books indexed in the Book Citation Index in Web of Science™ Core Collection (BKCI)

Interested in publishing with us?
Contact book.department@intechopen.com

Numbers displayed above are based on latest data collected.
For more information visit www.intechopen.com

6

Electrodynamical Modelling of Open Cylindrical and Rectangular Silicon Carbide Waveguides

L. Nickelson, S. Asmontas and T. Gric
Semiconductor Physics Institute of Center for Physical Sciences and Technology
Vilnius, Lithuania

1. Introduction

Silicon carbide (SiC) waveguides operating at the microwave range are presently being developed for advantageous use in high-temperature, high-voltage, high-power, high critical breakdown field and high-radiation conditions. SiC does not feel the impact of any acids or molten salts up to 800°C. Additionally SiC devices may be placed very close together, providing high device packing density for integrated circuits.
SiC has superior properties for high-power electronic devices, compared to silicon. A change of technology from silicon to SiC will revolutionize the power electronics. Wireless sensors for high temperature applications such as oil drilling and mining, automobiles, and jet engine performance monitoring require circuits built on the wide bandgap semiconductor SiC. The fabrication of single mode SiC waveguides and the measurement of their propagation loss is reported in (Pandraud et al., 2007).
There are not enough works proposing the investigations of SiC waveguides. We list here as an example some articles. The characteristics of microwave transmission lines on 4H-High Purity Semi-Insulating SiC and 6H, p-type SiC were presented as a function of temperature and frequency in (Ponchak et al, 2004). An investigation of the SiC pressure transducer characteristics of microelectromechanical systems on temperature is given in (Okojie et al., 2006). The high-temperature pressure transducers like this are required to measure pressure fluctuations in the combustor chamber of jet and gas turbine engines. SiC waveguides have also successfully been used as the microwave absorbers (Zhang, 2006).
The compelling system benefits of using SiC Schottky diodes, power MOSFETs, PiN diodes have resulted in rapid commercial adoption of this new technology by the power supply industry. The characteristics of SiC high temperature devices are reviewed in (Agarwal et al., 2006).
Numerical studies of SiC waveguides are described in an extremely limited number of articles (Gric et al., 2010; Nickelson et al., 2009; Nickelson et al., 2008). The main difficulty faced by researchers in theoretical calculations of the SiC waveguides is large values of material losses and their dependence on the frequency and the temperature. We would like to draw your attention to the fact that we take the constitutive parameters of the SiC material from the experimental data of article (Baeraky, 2002) at certain temperatures. Then for the frequency dependence, we take into account through the dependence of the

imaginary part of the complex permittivity of semiconductor SiC material on the specific resistivity and the frequency by the conventional formula (Asmontas et al., 2009).
We would like to underline also that there are theoretical methods for calculation of strong lossy waveguides, but these methods were usually used for the electrodynamical analysis of metamaterial waveguides (Smith et al., 2005; Chen et al., 2006; Asmontas et al, 2009; Gric et al., 2010; Nickelson et al., 2008) or other lossy material waveguides (Bucinskas et al., 2010; Asmontas et al., 2010; Nickelson et al., 2009; Swillam et al., 2008; Nickelson et al., 2008; Asmontas et al., 2006).
In this chapter we present the electrodynamical analysis of open rectangular and circular waveguides. The waveguide is called the open when there is no metal screen. In sections 2 and 3 we give a short description of the Singular Integral Equations' (SIE) method and of the partial area method that we have used to solve the electrodynamical problems. Our method SIE for solving the Maxwell's equations is pretty universal and allowed us to analyze open waveguides with any arbitrary cross-sections in the electrodynamically rigorously way (by taking into account the edge condition and the condition at infinity). The false roots did not occur applying the SIE method. The waveguide media can be made of strongly lossy materials.
In order to determine the complex roots of the waveguide dispersion equations we have used the Müller's method. All the algorithms have been tested by comparing the obtained results with the results from some published sources. Some of the comparisons are presented in section 4.
Both of the methods allow solving Maxwell's equations rigorously and are suitable for making the full electrodynamical analysis. We are able to calculate the dispersion characteristics including the losses of all the modes propagating in the investigated waveguide and the distributions of the electromagnetic (EM) fields inside and outside of the waveguides**.** We used our computer algorithms based on two mentioned methods with 3D graphical visualization in the MATLAB language.

2. The SIE method

In this section, we describe the SIE method for solving Maxwell's equations in the rigorous problem formulation (Nickelson et al., 2009; Nickelson & Shugurov, 2005). Using the SIE method, it is possible to rigorously investigate to investigate the dispersion characteristics of main and higher modes in regular waveguides of arbitrary cross–section geometry containing piecewise homogeneous materials as well as the distribution of the EM field inside and outside of waveguides electrodynamically..
Our proposed method consists of finding the solution of differential equations with a point–source. Then the fundamental solution of the differential equations is used in the integral representation of the general solution for each particular boundary problem. The integral representation automatically satisfies Maxwell's differential equations and has the unknown density functions μ_e and μ_h, which are found using the proper boundary conditions. To present the fields in the integral form we use the solutions of Maxwell's equations with electric $\vec{j}_e$ and magnetic $\vec{j}_h$ point sources:

$$\mathrm{Curl}\,\vec{E} = -\mu_0\mu_r\frac{\partial\vec{H}}{\partial t} - \vec{j}_h, \qquad \mathrm{Curl}\,\vec{H} = \varepsilon_0\varepsilon_r\frac{\partial\vec{E}}{\partial t} - \vec{j}_e \tag{1}$$

where $\vec{E}$ is the electric field strength vector and $\vec{H}$ is the magnetic field strength vector. Also ε_r is the relative permittivity and μ_r is the relative permeability of the medium. The electric and magnetic constants ε_0, μ_0 are called the permittivity and the permeability of a vacuum. The dependence on time t and on the longitudinal coordinate z are assumed in the form $\exp(i(\omega t - hz))$. Here h=h'-h''i is the complex longitudinal propagation constant, where h' is the real part (phase constant), h'=2π/λ_w, λ_w is the wavelength of investigated mode and h'' is the imaginary part (attenuation constant). The magnitude ω=2πf is the cyclic operating frequency and i is the imaginary unit (i^2=-1). Because of the equations linearity the general solution is a sum of solutions when $\vec{j}_h \neq 0$, $\vec{j}_e = 0$ and $\vec{j}_h = 0$, and $\vec{j}_e \neq 0$. The transversal components E_x, E_y, H_x, H_y of the EM field are being expressed through the longitudinal components E_z, H_z of EM field from Maxwell's equations as follows:

$$E_x = \frac{\mu_0\mu_r i\omega \frac{\partial H_z}{\partial y} + ih\frac{\partial E_z}{\partial x}}{\Delta},\quad E_y = \frac{-\mu_0\mu_r i\omega \frac{\partial H_z}{\partial x} + ih\frac{\partial E_z}{\partial y}}{\Delta}, \tag{2}$$

$$H_x = \frac{-\varepsilon_0\varepsilon_r i\omega \frac{\partial E_z}{\partial y} + ih\frac{\partial H_z}{\partial x}}{\Delta},\quad H_y = \frac{\varepsilon_0\varepsilon_r i\omega \frac{\partial E_z}{\partial x} + ih\frac{\partial H_z}{\partial y}}{\Delta}, \tag{3}$$

where $\Delta = h^2 - k^2\varepsilon_r\mu_r$.

The longitudinal components E_z, H_z, satisfy scalar wave equations, which are Helmholtz's equations:

$$\left(\Delta_\perp + k_\perp^2\right)H_Z = 0, \qquad \left(\Delta_\perp + k_\perp^2\right)E_Z = 0, \tag{4}$$

here $\Delta_\perp = \frac{\partial^2}{\partial x^2} + \frac{\partial^2}{\partial y^2}$ is the transversal Laplacian. Other magnitudes are $k_\perp^2 = -\Delta = k^2\varepsilon_r\mu_r - h^2$, k=ω/c and c is the light velocity in a vacuum. The fundamental solution of the second order differential equations (4) in the cylindrical coordinates (or in the polar coordinates, since the dependence on the longitudinal coordinate has already been determined) is the Hankel function of the zeroth order.

In Fig. 1 the points of the contour L where we satisfy the boundary conditions on the boundary line, dividing the media with the constitutive parameters of SiC: ε_r^{SiC}, μ_r^{SiC} and an environment area ε_r^a, μ_r^a are shown.

The problem is formulated in this way. We have in the complex plane a piecewise smooth contours L (Fig.1). The contour subdivides the plane into two areas; the inner S^+ and the outer S^- one. These areas according to the physical problem are characterized by different electrophysical parameters: the area S^+ has the constitutive parameters ε_r^{SiC}, μ_r^{SiC} and S^- has the constitutive parameters ε_r^a, μ_r^a of ambient air. Magnitudes ε_r^{SiC} = Re (ε_r^{SiC}) – Im (ε_r^{SiC}) and

μ_r^{SiC} = Re (μ_r^{SiC}) - Im (μ_r^{SiC}) are the complex permittivity and the complex permeability of the SiC medium. The positive direction of going round the contour is when the area S^+ is on the left side.

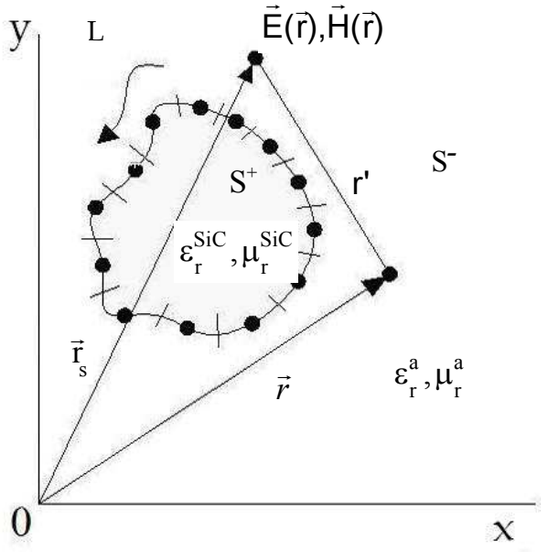

Fig. 1. Waveguide arbitrary cross section and designations for explaining the SIE method.

One has to determine in area S^+ solutions of Helmholtz's equation (4), which satisfy the boundary conditions for the tangent components of the electric and magnetic fields:

$$E^+_{tan}\big|_L = E^-_{tan}\big|_L , \tag{5}$$

$$H^+_{tan}\big|_L = H^-_{tan}\big|_L . \tag{6}$$

In the present work all boundary conditions are satisfied including the edge condition at the angular points of the waveguide cross-section counter and the condition at infinity.
The longitudinal components of the electric field and the magnetic field at the contour points that satisfied to the Helmholtz's equations (4) have the form:

$$E_z(\vec{r}) = \int_L \mu_e(\vec{r}_s) H_0^{(2)}(k_\perp r')ds, \tag{7}$$

$$H_z(\vec{r}) = \int_L \mu_h(\vec{r}_s) H_0^{(2)}(k_\perp r')ds, \tag{8}$$

where $E_z(\vec{r})$, $H_z(\vec{r})$ are the longitudinal components of the electric field and the magnetic field of the propagating microwave. Here $\vec{r} = \vec{i}x + \vec{j}y$ is the radius vector of the point, where the EM fields are determined, where $\vec{i}, \vec{j}$ are the unit vectors. The magnitudes $\mu_e(\vec{r}_s)$ and

$\mu_h(\vec{r}_s)$ are the unknown functions satisfying Hölder condition (Gakhov, 1977). Here $H_0^{(2)}(k_\perp r')$ is the Hankel function of the zeroth order and the second kind, where $r' = |\vec{r}_s - \vec{r}|$. The magnitude $\vec{r}_s = \vec{i}x_s + \vec{j}y_s$ is the radius vector (Fig. 1). Here ds is an element of the contour L and the magnitude s is the arc abscissa.

The expressions of all the electric field components which satisfy the boundary conditions are presented below. We apply the Krylov–Bogoliubov method whereby the contour L is divided into n segments and the integration along a contour L is replaced by a sum of integrals over the segments j=1…n. The expressions of all electric field components for the area S^+ and S^- are presented below:

$$E_z^+ = \sum_{j=1}^{n} \mu_e^+(s_j) \int_{\Delta L} H_0^{(2)}(k_\perp^+ r')ds\,, \tag{9}$$

$$E_z^- = \sum_{j=1}^{n} \mu_e^-(s_j) \int_{\Delta L} H_0^{(2)}(k_\perp^- r')ds\,. \tag{10}$$

We obtain that the transversal components of the electric field E_x, E_y after substituting formula (9) and (10) in the formulae (2) are:

$$\begin{aligned}\left(E_x\right)^+ = &-\left(i\mu_0\mu_r^{SiC}\omega \Big/ \left(k_\perp^+\right)^2\right)\left[k_\perp^+ \sum_{j=1}^{n}\left(\mu_h^+(s_j)\right)\int_{\Delta L} H_1^{(2)}(k_\perp^+ r')\frac{y_s - y_0}{r'}ds\right] \\ &+\left(ih \Big/ \left(k_\perp^+\right)^2\right)\left[k_\perp^+ \sum_{j=1}^{n}\left(\mu_e^+(s_j)\right)\int_{\Delta L} H_1^{(2)}(k_\perp^+ r')\frac{x_s - x_0}{r'}ds\right] - \frac{2\mu_0\mu_r^{SiC}\omega\cos\theta}{\left(k_\perp^+\right)^2}\mu_h^+(s_j),\end{aligned} \tag{11}$$

$$\begin{aligned}\left(E_y\right)^+ = &-\left(ih \Big/ \left(k_\perp^+\right)^2\right)\left[k_\perp^+ \sum_{j=1}^{n}\left(\mu_e^+(s_j)\right)\int_{\Delta L} H_1^{(2)}(k_\perp^+ r')\frac{y_s - y_0}{r'}ds\right] \\ &-\left(i\mu_0\mu_r^{SiC}\omega \Big/ \left(k_\perp^+\right)^2\right)\left[k_\perp^+ \sum_{j=1}^{n}\left(\mu_h^+\left(s_j\right)\right)\int_{\Delta L} H_1^{(2)}(k_\perp^+ r')\frac{x_s - x_0}{r'}ds - \frac{2\mu_0\mu_r^{SiC}\omega\cos\theta}{\left(k_\perp^+\right)^2}\mu_h^+(s_j),\right.\end{aligned} \tag{12}$$

$$\begin{aligned}\left(E_x\right)^- = &-\left(i\mu_0\mu_r^a\omega \Big/ \left(k_\perp^-\right)^2\right)\left[k_\perp^- \sum_{j=1}^{n}\left(\mu_h^-\left(s_j\right)\right)\int_{\Delta L} H_1^{(2)}(k_\perp^- r')\frac{y_s - y_0}{r'}ds\right] \\ &+\left(ih \Big/ \left(k_\perp^-\right)^2\right)\left[k_\perp^- \sum_{j=1}^{n}\left(\mu\bar{e}(s_j)\right)\int_{\Delta L} H_1^{(2)}(k_\perp^- r')\frac{x_s - x_0}{r'}ds\right] + \frac{2\mu_0\mu_r^a\omega\cos\theta}{\left(k_\perp^-\right)^2}\mu_h^-(s_j),\end{aligned} \tag{13}$$

$$\left(E_y\right)^{-} = -\left(ih\Big/\left(k_\perp^{-}\right)^2\right)\left[k_\perp^{-}\sum_{j=1}^{n}\left(\mu_e^{-}(s_j)\right)\int_{\Delta L} H_1^{(2)}(k_\perp^{-}r')\frac{y_s - y_0}{r'}ds\right] \tag{14}$$

$$-\left(\left(i\mu_0\mu_r^a\omega\right)\Big/\left(k_\perp^{-}\right)^2\right)\left[k_\perp^{-}\sum_{j=1}^{n}\left(\mu_h^{-}(s_j)\right)\int_{\Delta L} H_1^{(2)}(k_\perp^{-}r')\frac{x_s - x_0}{r'}ds\right] + \frac{2\mu_0\mu_r^a\omega\cos\theta}{\left(k_\perp^{-}\right)^2}\mu_h^{-}(s_j).$$

The field components and the values of the functions $\mu_e(s_j)$ and $\mu_h(s_j)$ are noted in the upper–right corner with the sign corresponding to different waveguide area, for instance, the functions $\mu_e^{+}(s_j)$, $\mu_h^{+}(s_j)$ or $\mu_e^{-}(s_j)$, $\mu_h^{-}(s_j)$ (Fig.1). These functions at the same contour point are different for the field components in the areas S^{+} and S^{-}, i.e. $\mu_h^{+}(s_j) \neq \mu_h^{-}(s_j)$. The magnitude $H_0^{(2)}$ is the Hankel function of the zeroth order and of the second kind, $H_1^{(2)}$ is the Hankel function of the first order and of the second kind. Here $k_\perp^{+} = \sqrt{k^2\varepsilon_r^{SiC}\mu_r^{SiC} - h^2}$ and $k_\perp^{-} = \sqrt{h^2 - k^2\varepsilon_r^a\mu_r^a}$ are the transversal propagation constants of the SiC medium in the area S^{+} and in the air area S^{-}, correspondingly (Fig.1). The segment of the contour L is $\Delta L = L/n$, where the limits of integration in the formulae (9-14) are the ends of the segment ΔL. The angle θ is equal to g 90° with g from 1 to 4, if the contour of the waveguide cross-section is a rectangular one, then the result can be $\cos\theta = \pm 1$ and $\sin\theta = \pm 1$ in the formulae (11-14).
We obtain the transversal components of the magnetic field H_x and H_y using SIE method in the form analogical formulae (9) – (12) after substituting formula (8) in the formulae (3).
After we know all EM wave component representations in the integral form we substitute the component representations to the boundary conditions (5) and (6). We obtain the homogeneous system of algebraic equations with the unknowns $\mu_e^{+}(s_j)$, $\mu_h^{+}(s_j)$, $\mu_e^{-}(s_j)$ and $\mu_h^{-}(s_j)$. The condition of solvability is obtained by setting the determinant of the system equal to zero. The roots of the system allowed us to determine the complex propagation constants of the main and higher modes of the waveguide. After obtaining the propagation constant of some required mode, the determination of the electric and magnetic fields of the mode becomes possible. For the correct formulated problem (Gakhov, 1977) the solution is one–valued and stable with respect to small changes of the coefficients and the contour form (Nickelson & Shugurov, 2005).

3. The partial area method

The presentation of longitudinal components of the electric E_z^{SiC} and magnetic H_z^{SiC} fields that satisfies Maxwell's equations in the SiC medium (Nickelson et al., 2008; Nickelson et al., 2007) are as follows:

$$E_z^{SiC} = A_1 J_m\left(k_\perp^{+} r\right)\exp(im\varphi), \quad H_z^{SiC} = B_1 J_m\left(k_\perp^{+} r\right)\exp(im\varphi), \tag{15}$$

where J_m is the Bessel function of the m−th order, A_1 and B_1 are unknown arbitrary amplitudes. The longitudinal components of the electric field E_z^a and the magnetic field H_z^a that satisfy Maxwell's equations in the ambient waveguide medium (in air) are as follows:

$$E_z^a = A_2 H_m^{(2)}\left(k_\perp^- r\right)\exp(im\varphi)\ ,\ H_z^a = B_2 H_m^{(2)}\left(k_\perp^- r\right)\exp(im\varphi), \tag{16}$$

where A_2 and B_2 are unknown arbitrary amplitudes, $H_m^{(2)}$ is the Hankel function of the m−th order and the second kind, r is the radius of the circular SiC waveguide, m is the azimuthal index characterizing azimuthal variations of the field, φ is the azimuthal angle.
A further solution is carried out under the scheme of section 2 of present work. The resulting solution is the dispersion equation in the determinant form:

$$\begin{gathered}
A_1 J_m\left(k_\perp^+ r\right) - A_2 H_m^{(2)}\left(k_\perp^- r\right) = 0,\\
B_1 J_m\left(k_\perp^+ r\right) - B_2 H_m^{(2)}\left(k_\perp^- r\right) = 0,\\
\frac{mh}{\left(k_\perp^+\right)^2 r} A_1 J_m\left(k_\perp^+ r\right) + \frac{i\omega\mu_0\mu_r^{SiC}}{k_\perp^+} B_1 J_m'\left(k_\perp^+ r\right)\\
-\frac{mh}{\left(k_\perp^-\right)^2 r} A_2 H_m^{(2)}\left(k_\perp^- r\right) - \frac{i\omega\mu_0\mu_r^a}{k_\perp^-} B_2\left(H_m^{(2)}\left(k_\perp^- r\right)\right)' = 0\ ,\\
\frac{mh}{\left(k_\perp^+\right)^2 r} B_1 J_m\left(k_\perp^+ r\right) - \frac{i\omega\varepsilon_0\varepsilon_r^{SiC}}{k_\perp^+} A_1 J_m'\left(k_\perp^+ r\right)\\
-\frac{mh}{\left(k_\perp^-\right)^2 r} B_2 H_m^{(2)}\left(k_\perp^- r\right) + \frac{i\omega\varepsilon_0\varepsilon_r^a}{k_\perp^-} A_2\left(H_m^{(2)}\left(k_\perp^- r\right)\right)' = 0.
\end{gathered} \tag{17}$$

We have used the Müller's method to find the complex roots. The roots of the dispersion equation give the propagation constants of waveguide modes. After obtaining the propagation constants of desired modes we can determine the EM field of these modes.

4. Validation of the computer softwares

We validated all our algorithms. Some of the validation results are presented in this section. We have created the computer software based on the method SIE (Section 2) in the MATLAB language. This software let us calculate the dispersion characteristics of waveguides with complicated cross-sectional shapes as well as the 3D EM field distributions. The computer software was validated by comparison with data from different

published sources, for example, the dispersion characteristics of the rectangular dielectric waveguide (Ikeuchi et al., 1981) and the modified microstrip line (Nickelson & Shugurov, 2005). In Figs. 2 and 3 we see that an agreement of the compared results is very good. In Fig. 2 the dispersion characteristics of the rectangular waveguide with sizes $(15x5)\cdot10^{-3}$ m and the waveguide material permittivity equal to 2.06 are presented. Our calculations are the solid lines and the results from (Ikeuchi et al., 1981) are presented with points.
The dimensions of the microstrip line (Fig. 3) are given by: $d=3.17\cdot10^{-3}$ m, $w=3.043\cdot10^{-3}$ m, $l_1=l_2=5\cdot10^{-3}$ m, $t=3\cdot10^{-6}$ m. The permittivity of the microstrip line substrate is 11.8.

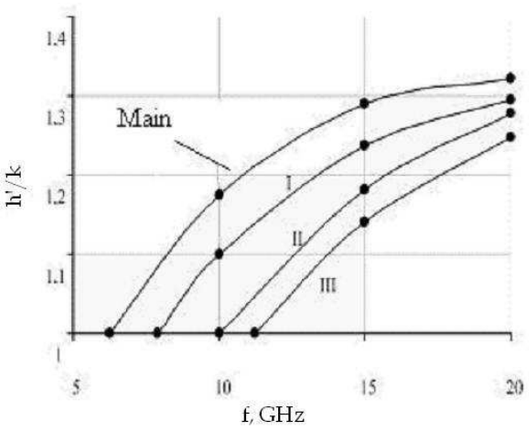

Fig. 2. Comparison of the dispersion characteristics of the rectangular dielectric waveguide calculated by SIE algorithm presented here and data from (Ikeuchi et. al., 1981)

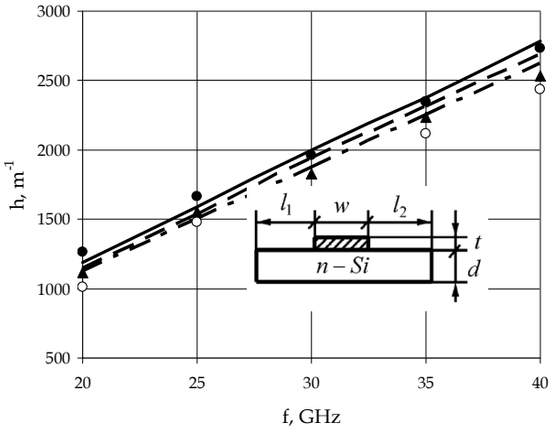

Fig. 3. Comparison of the microstrip line dispersion characteristics calculated by SIE algorithm and data from (Nickelson & Shugurov, 2005).

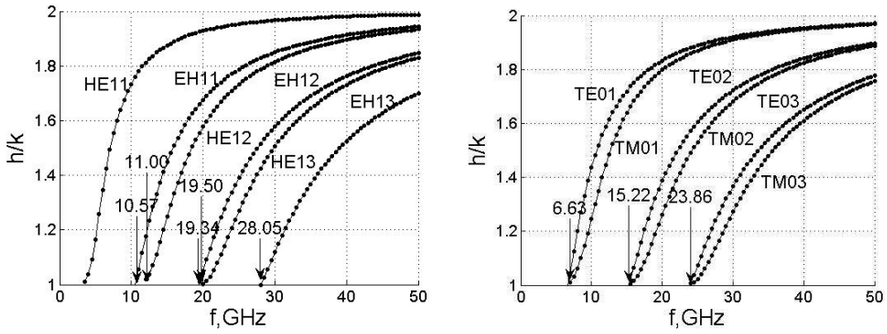

Fig. 4. The dispersion characteristics of the circular cylindrical dielectric waveguide: (a) – the hybrid modes and (b) – the axis-symmetric modes. The results taken from (Kim, 2004) are presented with solid lines and our calculations are presented with points.

In Fig. 3 our calculations are shown with dots (the main mode), with triangles (the first higher mode) and with circles (the second higher mode). In Fig. 3 the data from the book (Nickelson & Shugurov, 2005) is shown by the solid line (the main mode), dashed line (the first higher mode), dash-dotted line (the second higher mode).

We have also created the computer software on the basis of the partial area method **(**section 3) in the MATLAB language for calculations of the dispersion characteristics and the 2D &3D EM field distributions of circular waveguides. This software was validated by comparison with data from different published sources, for example, with (Kim, 2004). In Fig. 4 are shown dispersion characteristics of the circular cylindrical dielectric waveguide with a radius equal to 10^{-2} m and the permittivity of the dielectric equal to 4. In Fig. 4 (a) is shown six modes with the azimuth index m=1, are presented and in Fig 4 (b) six modes with the azimuth index m=0 are given. In Fig. 4. we see the good agreement between the simulations and the experimental results.
In Fig. 5 we demonstrate the validation of our computer program for calculations of the EM fields. We see that in work by (Kajfez & Kishk, 2002) the distribution of the electric field was presented by the arrows whose lengths are proportional to the intensity of the electric field at different points (Fig. 5(a)).

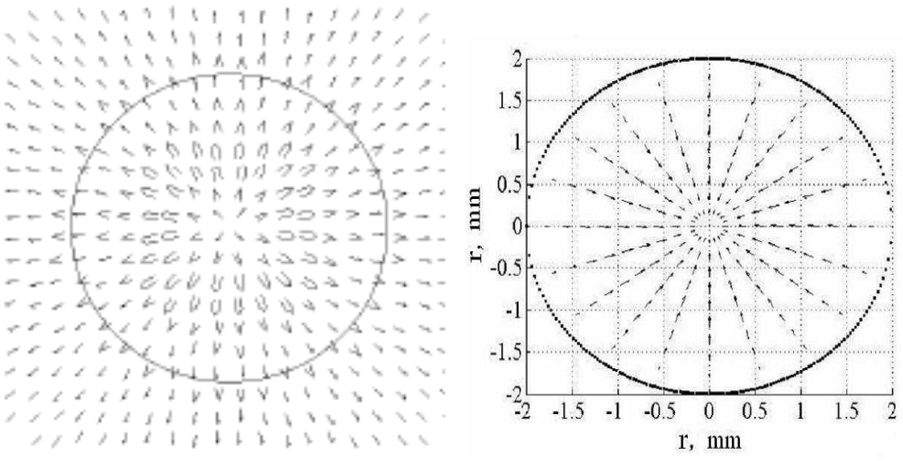

(a) (b)

Fig. 5. The electric field distributions of the TM_{01} mode propagating in the dielectric waveguide: (a) – (Kajfez & Kishk 2002) and (b) – our calculations are presented by the strength lines

In our electric field distribution, the electric field strength lines are proportional to the electric field intensity and also have directions. As far as the TE_{01} mode is characterized by the azimuth index m = 0, we should not see any variations of the electric field by the radius. In Fig. 5 (b) we see that the electric field has the radial nature and there are no variations of the electric field along the circular the radius.
The validation of our computer programs was made for different types of the waves having the different number of variations by the radius and the different azimuthal index. The distributions of the electric fields of other modes are also correct. It should be noticed that we have validation our computer programs for calculation of losses in the waveguide slowly increasing the losses of the material from Im (ε_r) = 0 and Im (μ_r) = 0 up to the required values.

5. The rectangular SiC waveguide

In this chapter we present the investigations of the electrodynamical characteristics of the open waveguides using the algorithm that is described in Section 2. Here we present our

calculations of two SiC waveguides with different cross-sectional dimensions at different temperatures. We also present the distributions of the magnetic fields at the temperature of 500°C.

5.1. The investigation of the rectangular SiC waveguide with sizes $(2.5x2.5)\cdot10^{-3}$ m^2 at T=500°C

The dispersion characteristics of the rectangular SiC waveguide at the temperature 500 °C are presented in Fig. 6. The sizes of the rectangular SiC waveguide are 2.5x2.5 mm^2. The dispersion characteristics of the main mode are shown by solid lines. The dispersion characteristics of the first higher mode are shown by dashed lines. Here the complex longitudinal propagation constant is h = h'-h''i, the phase constant h' = Re (h) [rad/m] and the attenuation constant h'' = Im (h) determines the waveguide losses [rad/mm = 8.7dB/mm]. Here h'=2π/λ_w, where λ_w is the wavelength of the waveguide modes. In our calculations the azimuthal index is m = 1, because the main waveguide mode has the index equal to unity. The magnitude *k* is the wavenumber. The permittivity of the SiC material is 6.5 – 0.5i at the temperature 500°C and the frequency f = 1.41 GHz (Baeraky, 2002). The values of the permittivity depend upon frequency (Asmontas et al., 2009).

Concerning the fact that SiC is the material with large losses at certain temperatures and frequencies the complex roots of the dispersion equation were calculated by the Müller method.

In Fig. 6(a) we see that the main and the first higher modes are slow waves (because h'/k > 1. The dependencies of losses of the both modes propagating in the rectangular SiC waveguide on the frequency range are pretty intricate (Fig. 6 (b)). The main mode has three loss maxima. We discovered that the minimum of the losses of the main mode is approximately at f=59 GHz. The losses of the first higher mode have the larger value at the frequency of 59 GHz. It means that the first higher mode is strongly absorbed in the waveguide at this frequency. Fig. 6 (b) shows the excellent properties of SiC waveguide at f = 59 GHz for creation of some devices on the base of the main mode. The SiC waveguide could be used for creation of single-mode devices.

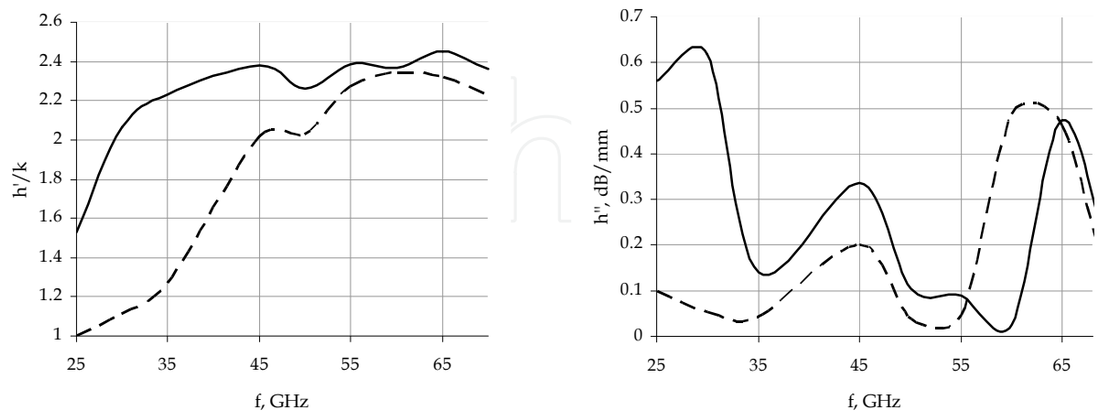

(a) (b)

Fig. 6. The dispersion characteristics of the rectangular SiC waveguide: (a) – the dependence of the normalized phase constant *h*'/k upon frequency and (b) - the dependence of the attenuation constant h'' upon frequency

The 3D magnetic field distribution of the main mode propagating in the rectangular SiC waveguide at T= 500°C and f=30 GHz is presented in Fig. 7.

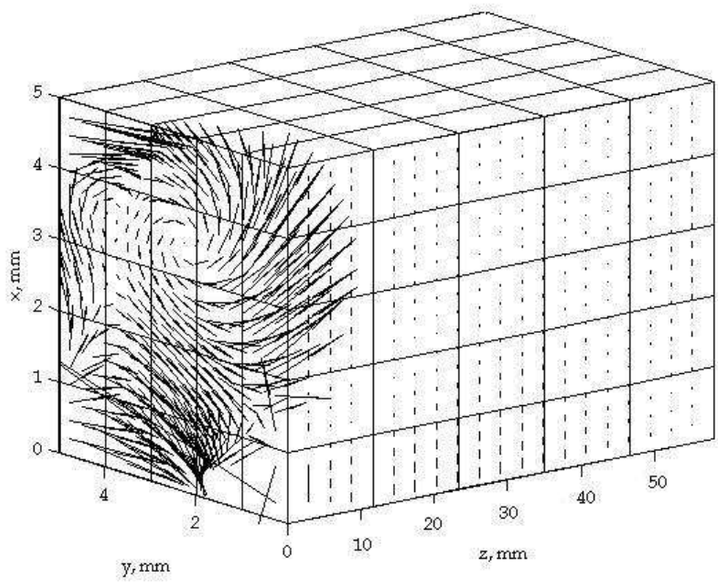

Fig. 7. The 3D vector magnetic field distribution of the main mode propagating in the open rectangular SiC waveguide at T= 500°C and f=30GHz

In Fig. 7 we see that the magnetic field of the main mode is distributed in the form of circles in the cross-section of the rectangular SiC waveguide. We can see the vertical magnetic field strength lines in the plane of a vertical waveguide wall along the z axis. The calculations were made with 100000 points in 3D space.

5.2 The investigation of the rectangular SiC waveguide with sizes $(3x3)\cdot10^{-3}$ m^2 at T=1000°C

The SiC waveguide with sizes $(3x3)\cdot10^{-3}$ m^2 has been analyzed at the temperature T = 1000°C (Fig. 8). The values of permittivities depend upon temperature and were taken from (Baeraky, 2002). The dispersion characteristics of the rectangular SiC waveguide are presented in Fig. 8.

In Fig. 8(a) are shown the phase constants of two modes propagating in the circular waveguide with the azimuth index m=1 (Nickelson & Gric, 2009). We see that the cutoff frequency of the main mode is 21 GHz and the first higher mode is 27 GHz. In Fig. 8 (b) we see the dependences of losses of the main and the first higher modes on frequency. We see that the loss dependences have the waving character. When the frequency is lower than 30 GHz, the losses of the main mode are larger than losses of the first higher mode at the same frequency interval. When the frequency is higher than 30 GHz, the losses of these modes have approximately the same values. Comparing the modes depicted in Fig. 8 with the analogue modes propagating in the circular dielectric waveguide, we should notice that the main mode is the hybrid HE_{11} mode and the first higher mode is the hybrid EH_{11} mode.

Comparing Figs. 6 and 8 we see that the dispersion characteristics can be changed by changing temperatures and waveguide cross-section sizes. Especially, we would stress that

the SiC waveguide operates in single-mode regime. And the waveguide broadband width is approximately 25%.

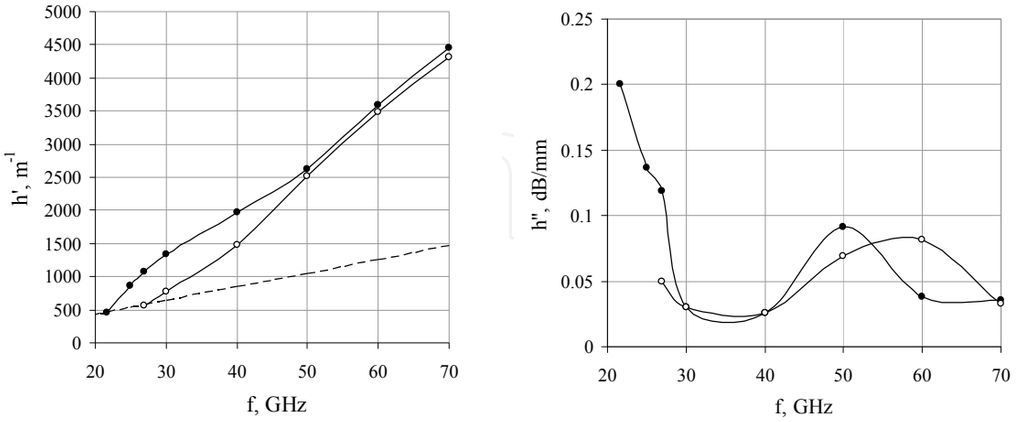

(a) (b)

Fig. 8. Dispersion characteristics of the main mode and the first higher mode of the rectangular SiC waveguide: (a) – dependence of the phase constants and (b) – dependence of the attenuation constants upon frequency. The main mode is denoted with points and the first higher mode is denoted with circles.

6. The circular SiC waveguide

Here we present the investigations of the electrodynamical characteristics of the open circular cylindrical waveguides using the algorithms presented in Chapter 3 (Gric et al., 2010; Asmontas et al., 2009; Nickelson et al., 2009; Nickelson et al. 2008). We propose our calculations of the dispersion characteristics of the SiC waveguide with different sizes of their cross-sections at several different temperatures. We also give here the 2D electric field distributions and the 3D magnetic field distributions.

6.1. The investigation of the circular cylindrical SiC waveguide with the radius 2.5 mm at three temperatures T=500°C, 1000°C and 1500°C

In Figs. 9 and 10 are presented the dispersion characteristics of the main and the first higher modes propagating in the open circular SiC waveguide at three different temperatures 500°C (solid line with crosses), 1000°C (solid line with black), 1500°C (solid line with circles). The permittivity of the SiC is 6.5 – 0.5i when T=500°C, 7-1i when T=1000°C and 8-2i when T=1500°C at f =11 GHZ. In Fig. 9(a) we see that the value of phase constant increases with increasing frequency. Comparing the dependence of the phase constant at 500°C, 1000°C and 1500°C we see that the higher the temperature is, the higher the values of the phase constant are.

The value of the attenuation constant increases with increasing the temperature and remains almost constant at frequencies above 20 GHz. This feature is important for operating of modulators and phase shifters which could be created on the basis of such waveguides. The EM signal propagating in the waveguide is not modulated by losses.

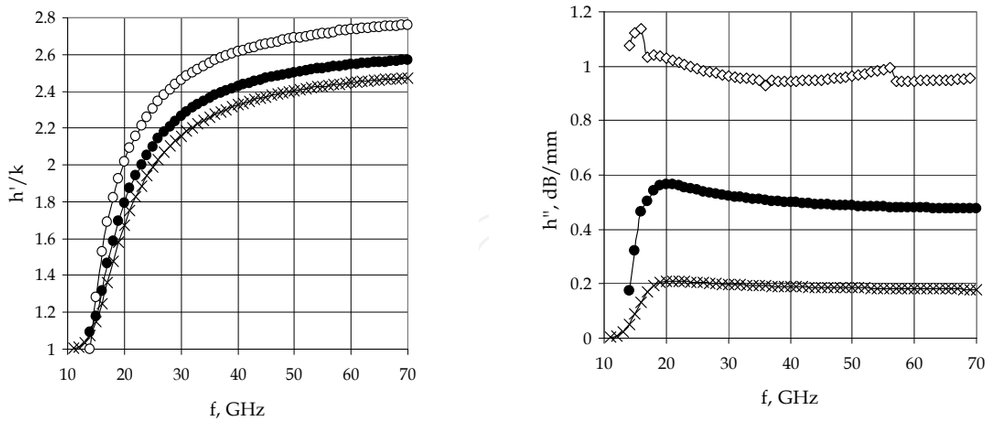

(a) (b)

Fig. 9. The dispersion characteristics of the main mode propagating in the circular SiC waveguide: (a) – the dependences of the normalized phase constant and (b)– the dependences of the attenuation constant upon the frequency at the temperatures 500°C, 1000°C and 1500°C.

In Fig. 10 we present the dispersion characteristics of the first higher modes propagating in the circular SiC waveguide at three different temperatures. We see from Fig. 10 (a) that at the low frequencies before 45 GHz the phase constant h' can be higher at the temperature 1000°C in comparison with h' at the temperatures 500°C and 1500°C. Thus the tendency of dependences of the complex longitudinal propagation constants upon frequency is destroyed for the first higher mode.

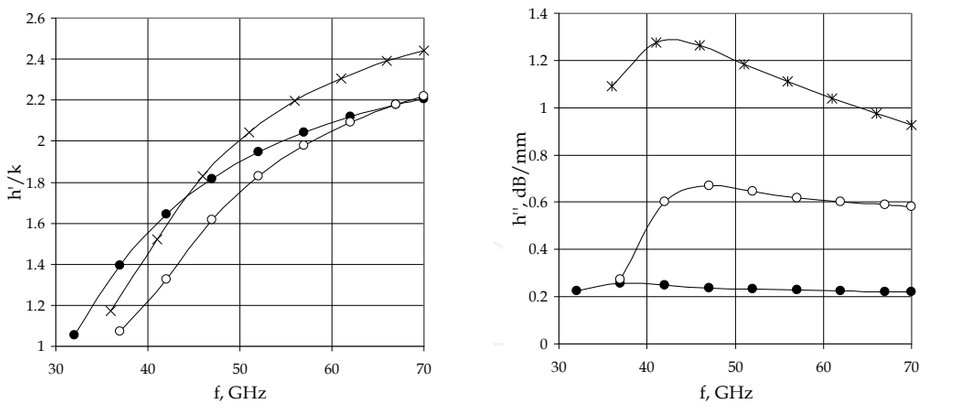

(a) (b)

Fig. 10. The dispersion characteristics of the first higher modes propagating in the circular SiC waveguide: (a) – the dependences of the normalized phase constant and (b) – the dependences of the attenuation constant upon the frequency at the temperatures 500°C, 1000°C, 1500°C

We see that the changes of attenuation constant curves (Fig. 10 (b) of the first higher mode are different compared to the same dependences of the main mode (Fig. 9(b)).

We have calculated all EM field components with 600 points inside and outside of the SiC waveguide. The 3D vector magnetic field distributions of the main mode propagating in the circular SiC waveguide at two temperatures 500°C and 1500°C and when f = 30 GHz are shown in Figs. 11 - 12. In Figs. 11(a) -12(a) the distribution of magnetic field lines in the waveguide cross-section as well as the magnetic field line projections on the vertical xOz and horizontal yOz planes in the longitudinal directions are shown. In Figs. 11(b) -12(b) the distributions of 3D vector magnetic field lines in the space of front quarter between the vertical xOz and horizontal yOz planes are presented. Calculations were fulfilled in the 300 points of every cross-section.

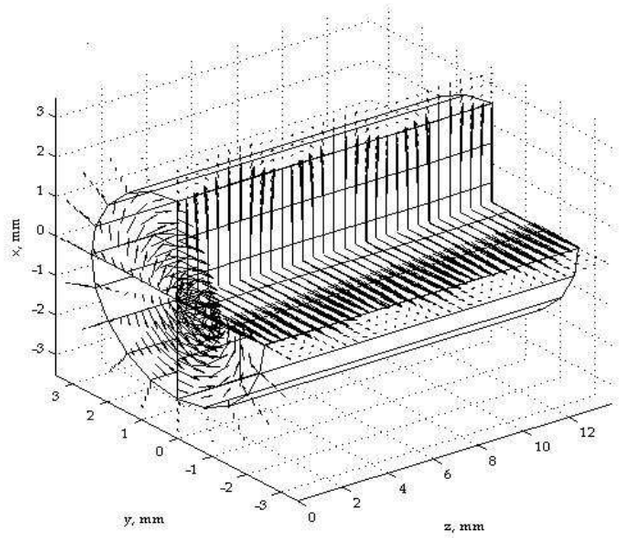

(a)

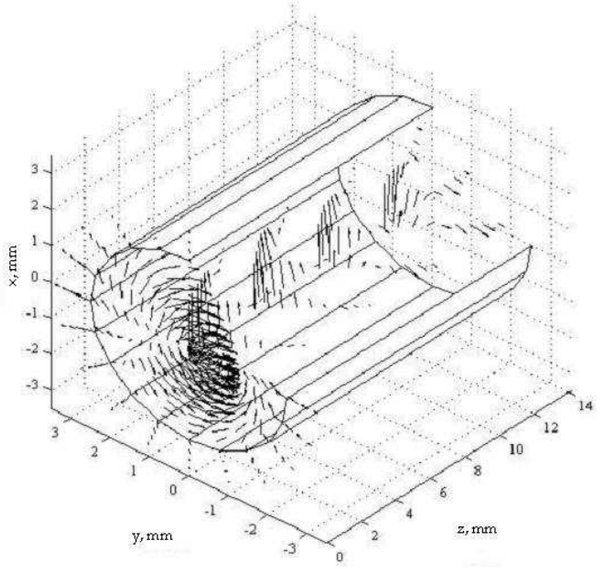

(b)

Fig. 11. The 3D vector magnetic field distributions of the main mode when T= 500 °C: (a) – the cross-section distribution of magnetic field lines as well as their projections at horizontal and vertical planes and (b) – the 3D vector magnetic field in the space of front quarter

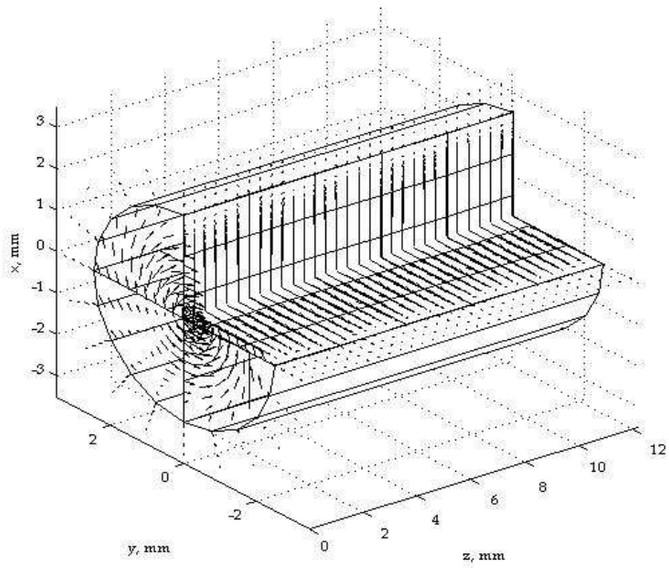

(a)

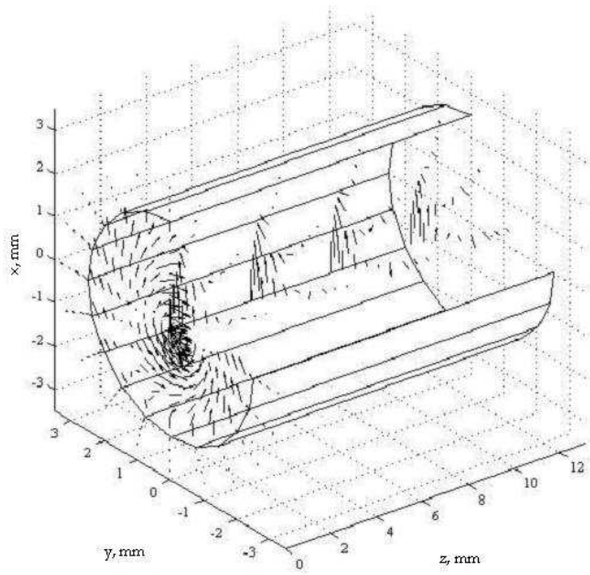

(b)

Fig. 12. The 3D vector magnetic field distributions of the main mode when T= 1500°C: (a) – the cross-section distribution of magnetic field lines as well as their projections at horizontal and vertical planes and (b) – the 3D vector magnetic field in the space of front quarter

The comparison of the magnetic fields at the temperatures 500°C, 1500°C (Fig. 11 and 12) shows that the magnetic field at 1500°C is weaker inside and outside of the waveguide. This happened due to the fact that the losses are larger at 1500°C.

6.2. The investigation of the circular SiC waveguide with radius 3 mm at T = 1000°C

Here we investigate the SiC rod waveguide (Nickelson et al., 2009). The radius of the SiC rod waveguide is 3 mm. The SiC waveguide has been analyzed at the temperature T = 1000°C. The permittivity of the SiC material at this temperature is 7-1i at f=11 GHz (Baeraky, 2002). The dependences of the phase constant and the attenuation constant of the SiC waveguide with the radius r=3 mm when T = 1000 °C on the operating frequency f are presented in Fig.13 (a) and (b).

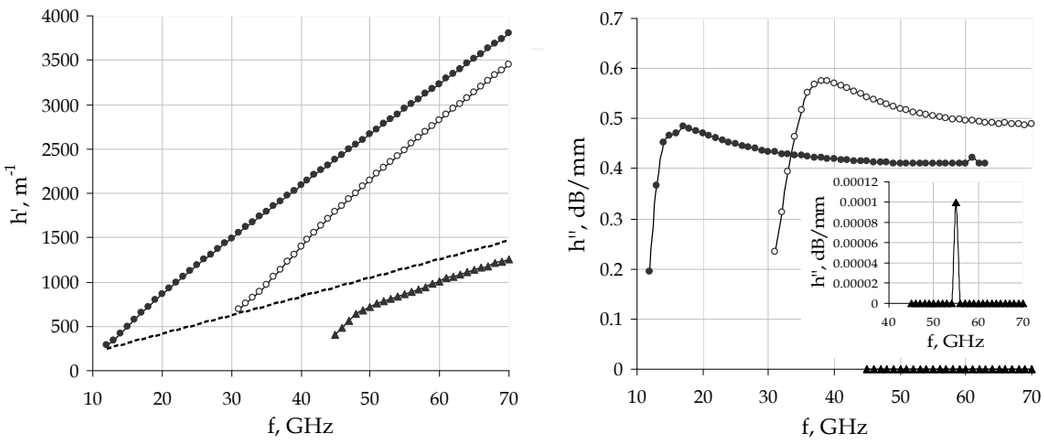

(a) (b)

Fig. 13. Dispersion characteristics of the SiC waveguide: (a) – dependence of the phase constants and (b) – dependence of the attenuation constant upon frequency. The main mode is denoted with points, the first higher mode is denoted with circles, the fast mode is denoted with triangles

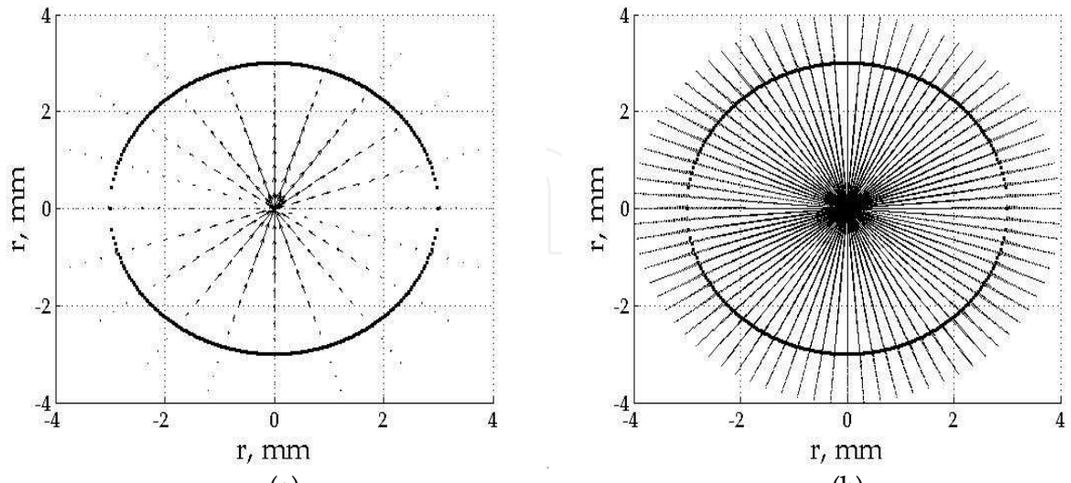

(a) (b)

Fig. 14. The electric field distribution of the main mode propagating in the SiC waveguide at f = 55 GHz: (a) – the electric fields strength lines and (b) – the electric field intensities

The electric field distributions of all the propagated modes were calculated at the frequency f = 55 GHz. The obtained results are presented in Figs. 14 - 16. Here we present the electric field strength lines and the electric field intensities. The intensity of the electric field is expressed through a module of the transversal electric field components.
In Fig. 14 we see that the electric field distribution of the main mode has one variation by radius. The strongest electric field of this mode concentrates in the centre of the waveguide at a small enough radius.

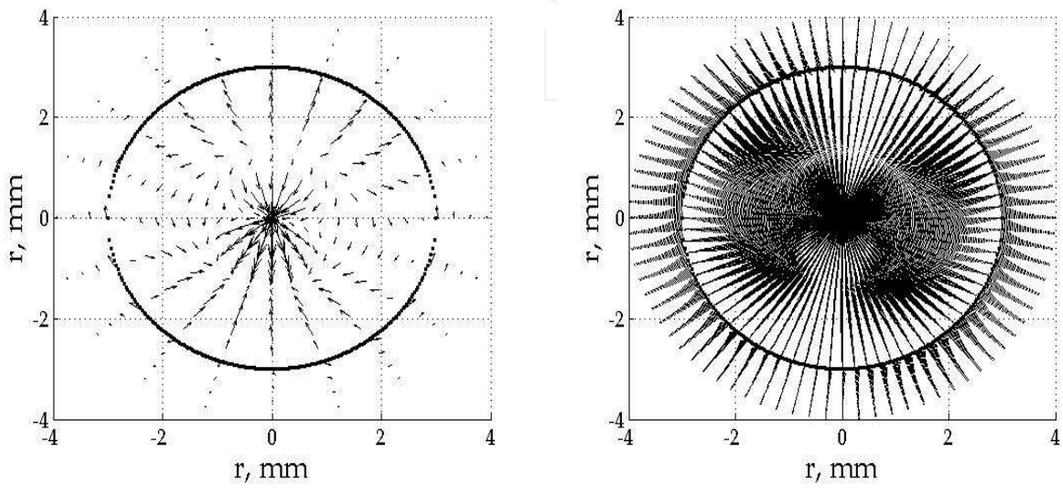

(a) (b)

Fig. 15. The electric field distribution of the first higher slow mode propagating in the SiC waveguide at f = 55 GHz: (a) – the electric fields strength lines and (b) – the electric field intensities

In Fig. 15 we see that the strongest electric field of this mode concentrates in the large part of the waveguide in the form of two twisted lobes.

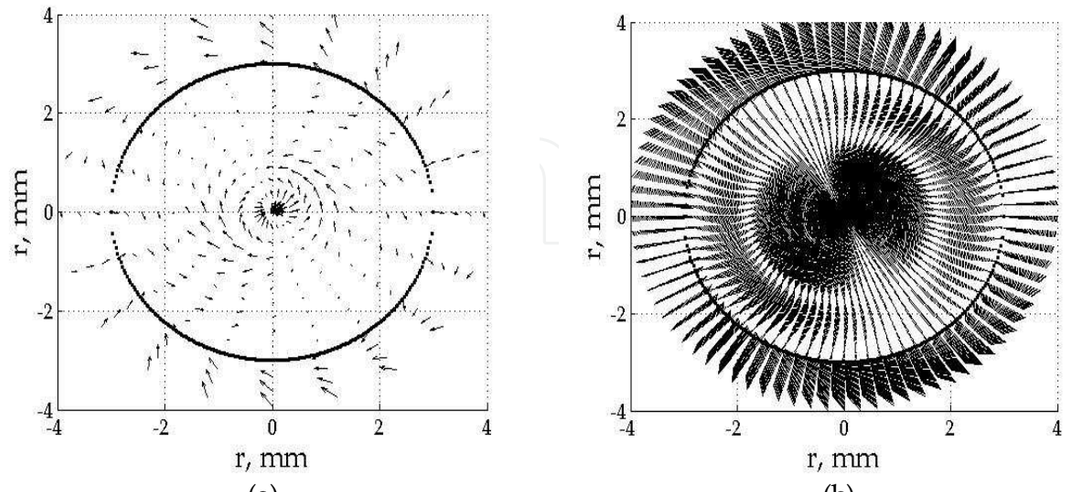

(a) (b)

Fig. 16. The electric field distribution of the second higher fast mode propagating in the SiC waveguide at f = 55 GHz: (a) – the electric fields strength lines and (b) – the electric field intensities

In Fig. 16 we see that the electric field distribution of the fast mode has two variations by radius. The strongest electric field of this mode concentrates in the centre of the waveguide in the form of two small lobes and outside it. We see that the electric field outside the waveguide is stronger in the places where the inner waveguide electric field is weaker.

6.3. The investigation of the circular SiC waveguide with radius 2.5 mm when T = 1800°C

The dependences of the phase constant and the attenuation constant of the SiC waveguide with the radius r=2.5 mm when T = 1800^{0}C on the operating frequency f are presented in Figs. 17 (a) and (b).

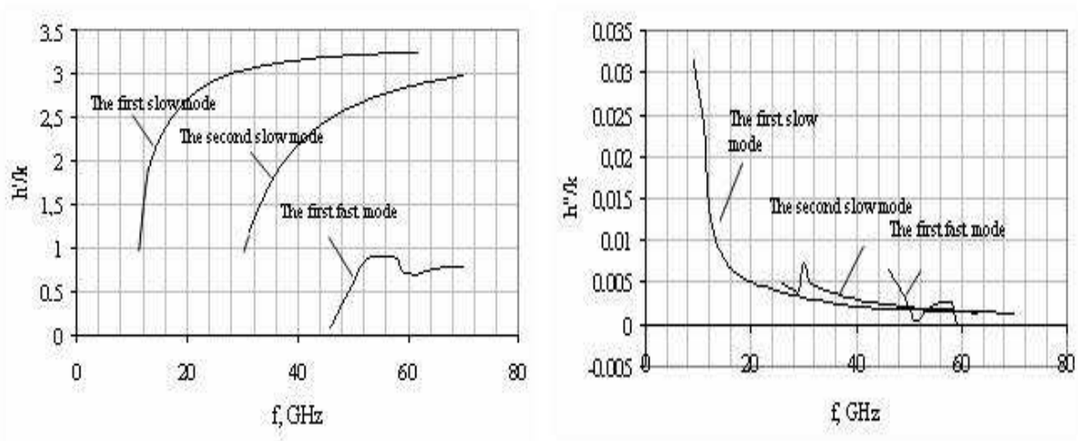

(a) (b)

Fig. 17. Dispersion characteristics of the SiC waveguide: (a) – dependence of the normalized phase constant and (b) – dependence of the normalized attenuation constant upon frequency

There are dispersion curves of three waveguide modes in Fig. 17. The main and first higher waveguide modes are slow modes, because their h′/k >1. The third depicted mode is a first fast mode because the value h′/k <1 for this mode.

The cutoff frequencies of the two slow modes are f_{cut}=12.5 GHz and 30 GHz respectively. The cutoff frequency of the first fast mode is f_{cut} = 46 GHz.

The propagation losses of all analyzed modes (see Fig. 17 (b)) were calculated in the assumption that the imaginary part of the complex permittivity Im (ε_r^{SiC}) is equal to 7 at the operating frequency 12.5 GHz. The value Im (ε_r^{SiC}) decreases when the operating frequency f increases, because this magnitude is inversely proportional to the value f (Asmontas et al., 2009). Analyzing the propagation losses of the slow and fast modes we see that the first slow mode has the largest propagation losses in the area of its cutoff frequency. We see peaks on the loss curves of the second and third modes. Our research has shown that the position of these peaks depends on the waveguide radius also. At smooth reduction of waveguide radius the peak of propagation losses will be smoothly displaced to the right side as a function of increasing frequencies.

The electric field distributions of the slow and fast modes are presented in Figs. 18 − 20. The distributions of the electric field were calculated in 10000 points. The electric field strength

lines are presented in Figs 18(a) − 20(a). Visualizations of the electric field intensity are shown in Figs 18(b) − 20(b).
The values of the electric E_r, E_φ, E_z and magnetic H_r, H_φ, H_z field components of these modes are summarized in Table 1.

Slow modes			
The main	m = 1, f = 15 GHz		
	E_r, V/m	E_φ, V/m	E_z, V/m
	$2.2 \cdot 10^{-2} - 8 \cdot 10^{-3}i$	$3.9 \cdot 10^{-2} + 4 \cdot 10^{-2}i$	$8 \cdot 10^{-2} + 1.46 \cdot 10^{-1}i$
	H_r, A/m	H_φ, A/m	H_z, A/m
	$-5.943 \cdot 10^{-4} - 6.49 \cdot 10^{-4}i$	$-1.6 \cdot 10^{-5} + 4.267 \cdot 10^{-5}i$	$4.148 \cdot 10^{-4} - 4.424 \cdot 10^{-4}i$
The first higher	m = 1, f = 50 GHz		
	E_r, V/m	E_φ, V/m	E_z, V/m
	$1.349 \cdot 10^{-4} - 1.582 \cdot 10^{-4}i$	$1.554 \cdot 10^{-4} + 1.204 \cdot 10^{-4}i$	$4.205 \cdot 10^{-4} + 3.623 \cdot 10^{-4}i$
	H_r, A/m	H_φ, A/m	H_z, A/m
	$-1.604 \cdot 10^{-6} - 1.127 \cdot 10^{-6}i$	$1.32 \cdot 10^{-6} - 1.643 \cdot 10^{-6}i$	$8.011 \cdot 10^{-7} - 1.115 \cdot 10^{-6}i$
Fast mode			
The second higher	m = 1, f = 51 GHz		
	E_r, V/m	E_φ, V/m	E_z, V/m
	$2.5 \cdot 10^{-2} - 1.4 \cdot 10^{-2}i$	$2 \cdot 10^{-2} - 1.6 \cdot 10^{-2}i$	$2.95 \cdot 10^{-1} - 3 \cdot 10^{-2}i$
	H_r, A/m	H_φ, A/m	H_z, A/m
	$-3.434 \cdot 10^{-4} + 6.650 \cdot 10^{-5}i$	$10^{-3} - 10^{-3}i$	$-2.887 \cdot 10^{-4} + 1.958 \cdot 10^{-4}i$

Table 1. The EM field components in the fixed point (r = 2.4 mm, φ=0, z=0) of the SiC waveguide cross-section when T = 1800^0C.

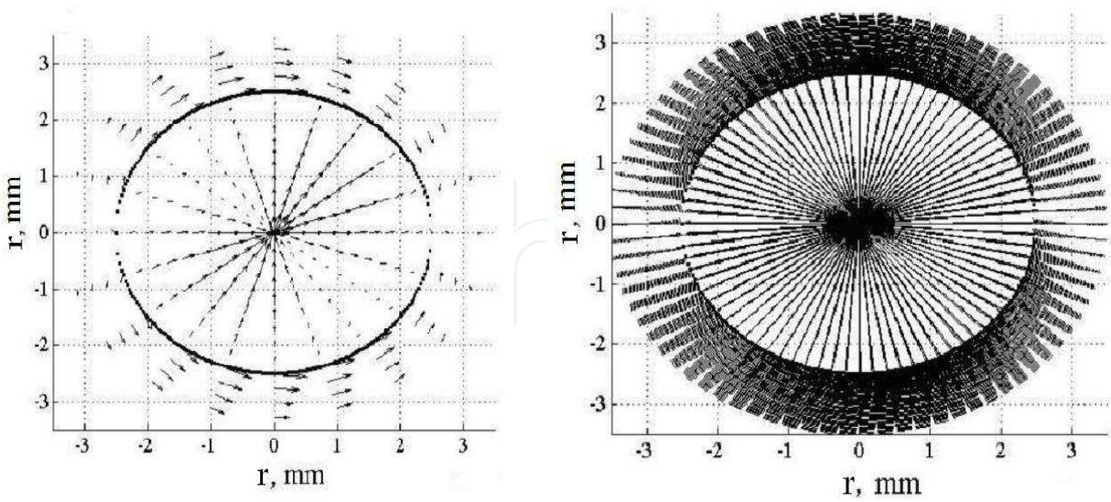

(a) (b)

Fig. 18. The electric field distribution of the first slow mode propagating in the SiC waveguide at f = 15 GHz: (a) – the electric fields strength lines and (b) – the electric field intensities

The electric field distributions of the first slow mode (the main mode) are presented in Fig. 18. We should notice that the electric field distribution of the first slow mode depicted in Fig. 18 (a) is rotated clockwise by 90 degrees respectively to the electric field distribution of the same mode propagated in the analogical waveguide made of lossless material SiC with Im (ε_r^{SiC})=0. In Fig. 18 (a) we can see that electric field strength lines are directed clockwise in the I and II quarters and counterclockwise in the III and IV quarters. The electric field strength lines are directed radially inside the SiC waveguide. We see that there is only one variation of the electric field on the waveguide radius. In Fig. 18 (b) we can see that the strongest electric field concentrates in the two areas. These ones are in the waveguide center and on the waveguide boundary. We see that the field is inhomogeneously distributed along the perimeter of the waveguide boundaries.

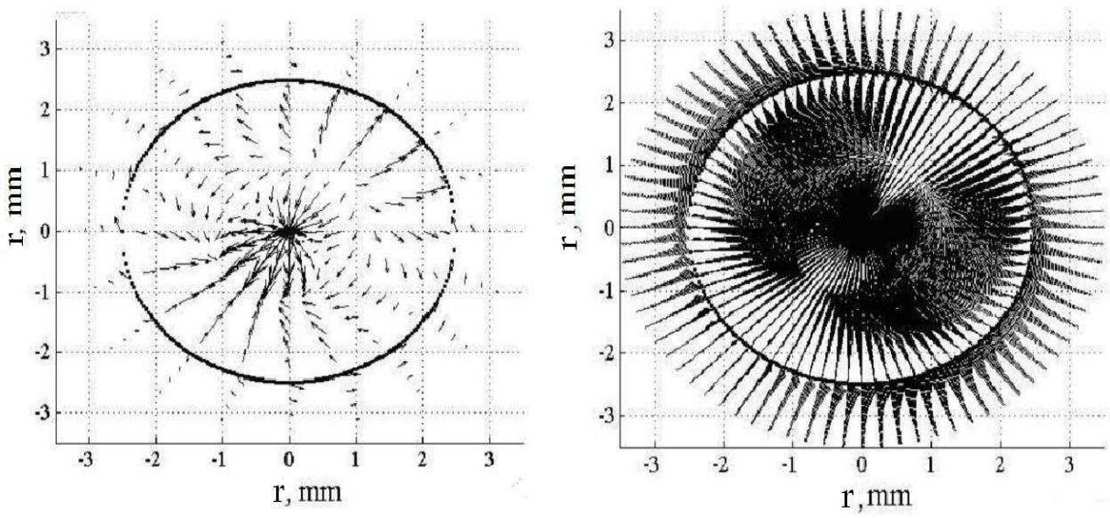

(a) (b)

Fig. 19. The electric field distribution of the second slow mode propagating in the SiC waveguide at f = 50 GHz: (a) – the electric fields strength lines and (b) – the electric field intensities

In Fig. 19 we can observe an interesting behavior of the electric field distribution of the second slow mode (the first higher waveguide mode) inside the SiC waveguide as well as outside it close to its boundary. In Fig. 19 (a) we see that there are two variations of the electric field on the waveguide radius. The electric field intensity distribution inside the waveguide has an intricate picture in the shape of two lobes. We see that when the distance from the waveguide becomes larger the electric field becomes smaller outside the waveguide. We should notice that there is a third slow mode (the third higher waveguide mode) in the frequency range of 1 – 100 GHz. The cutoff frequency of this mode is f_{cut} = 51 GHz. The third slow mode has two variations by the radius. The analysis of the third slow mode is beyond the present work.

In Fig. 20 we can see the electric field distribution of the first fast mode propagating in the SiC waveguide. The electric field strength lines of the first fast mode (the second higher waveguide mode that we study here) have three variations along the radius Fig. 20(a). In Fig. 20(b) we can observe that the electric field distribution of the first fast mode inside the

SiC waveguide is in the form of two lobes. The strongest electric field concentrates outside the waveguide. The number of variations of a field along the waveguide radius for all the modes corresponds to the current understanding about the main and higher modes of dielectric waveguides.

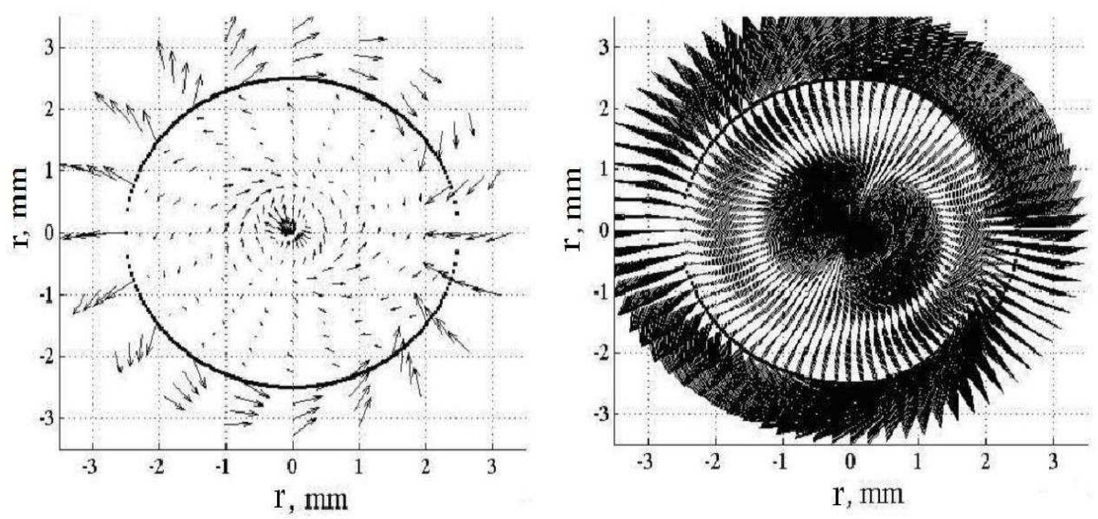

(a) (b)

Fig. 20. The electric field distribution of the first fast mode propagating in the SiC waveguide at f = 51 GHz: (a) – the electric fields strength lines and (b) – the electric field intensities

The comparison of Figs 18-20 shows us that the electric field distributions of different waveguide modes are strongly different.

7. The hollow-core SiC waveguide

The electrodynamical solution of the Helmholtz equation of analogical waveguides has already been presented in section 3 (Nickelson et al., 2008). We should mention that the argument of the Hankel function changes its sign if there is lossy material outside the waveguide.

The dispersion characteristics of the main and the first higher modes propagating in the hollow-core SiC waveguide with r = 1 mm at the temperatures T equal to 20°C, 1250°C, 1500°C, 1800°C are presented in Figs. 21 and 22.

In Fig. 21 we see the dependencies of the phase constant and the attenuation constant of the main mode on the frequency f. In Fig. 21(a) we see that the phase constants at temperatures T = 1250°C and T = 1500°C practically coincide. We can see that when the temperature decreases the cutoff frequencies of the main mode moves to the range of higher frequencies. The behavior of the attenuation constant (waveguide losses h'') are different at temperatures T = 1250°C and T = 1500°C (Fig. 21 (b)). The waveguide losses of the main modes became lower with increasing frequency until a certain value and after that losses started to increase again. We can see that the minima of waveguide losses at temperatures T = 20°C, 1250°C, 1500°C and 1800°C correspond to frequencies f = 118, 109, 79 and 56 GHz. The waveguide losses of the main modes (at different T) decrease in the beginning part of the dispersion

curves until their minima because the waveguide material has features of a polar dielectric in this frequency range. The waveguide losses of main modes increase after points of their minima because the waveguide material behaves as conductive media in this frequency range.

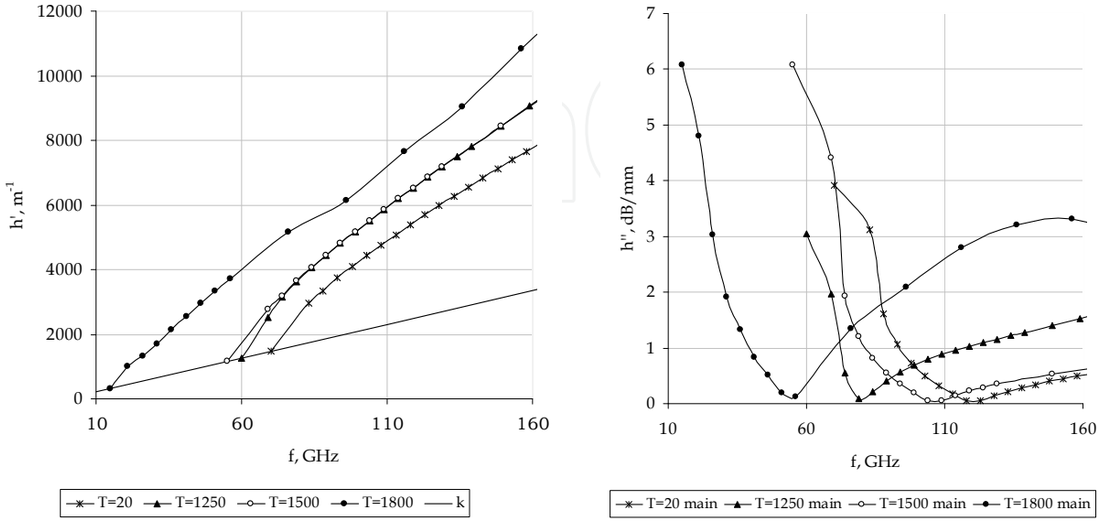

(a) (b)

Fig. 21. The complex dispersion characteristics of the main mode at the different temperatures

The dispersion characteristics of the first higher modes propagating in the hollow-core SiC waveguide with r = 1 mm at the different temperatures are presented in Fig. 22. We see that the behavior of waveguide losses at T = 1800°C is like for waveguide of conductive media.

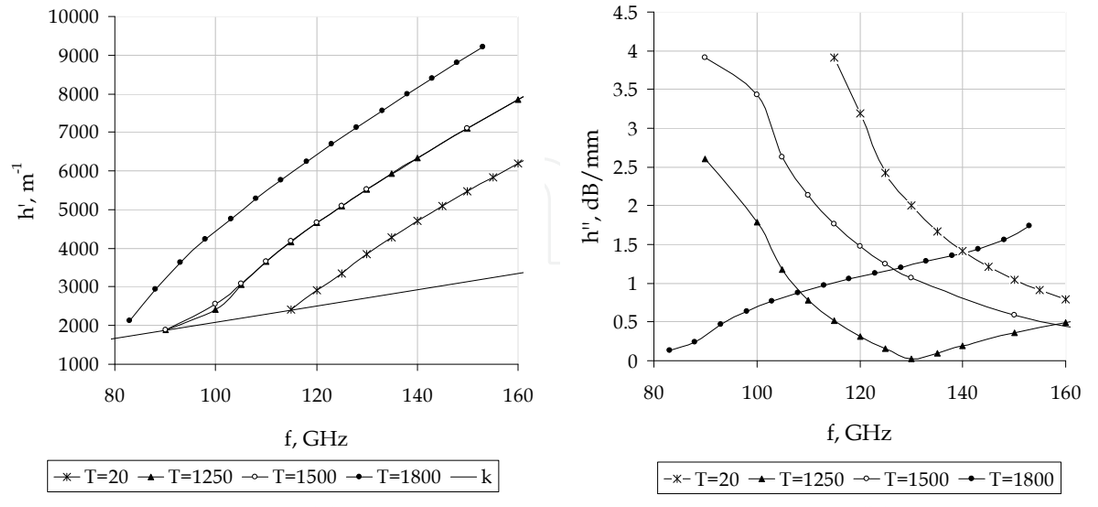

(a) (b)

Fig. 22. The complex dispersion characteristics of the first higher mode at the different temperatures

The features of the first higher mode losses at T = 20°C, 1250°C, 1500°C (Fig. 22b) can be explained in the same way as for the main mode (Fig. 21b).
The electric field distributions of the main hybrid HE_{11} mode and the first higher hybrid EH_{11} mode propagating in the hollow-core SiC waveguide at T = 20°C and 1800°C are presented, correspondingly, in Figs. 23, 24 and 25, 26. In all of these figures, the left side shows the electric field strength lines and the right (b) shows the intensity of the electric field. All electric field distributions were calculated at frequencies which are close to the cutoff frequencies of each investigated mode. The calculation of electric field in the waveguide cross-section was executed with 10000 points. We see from Figures 23 (a)-26 (a) that HE_{11} and EH_{11} modes have only one variation on the waveguide radius.

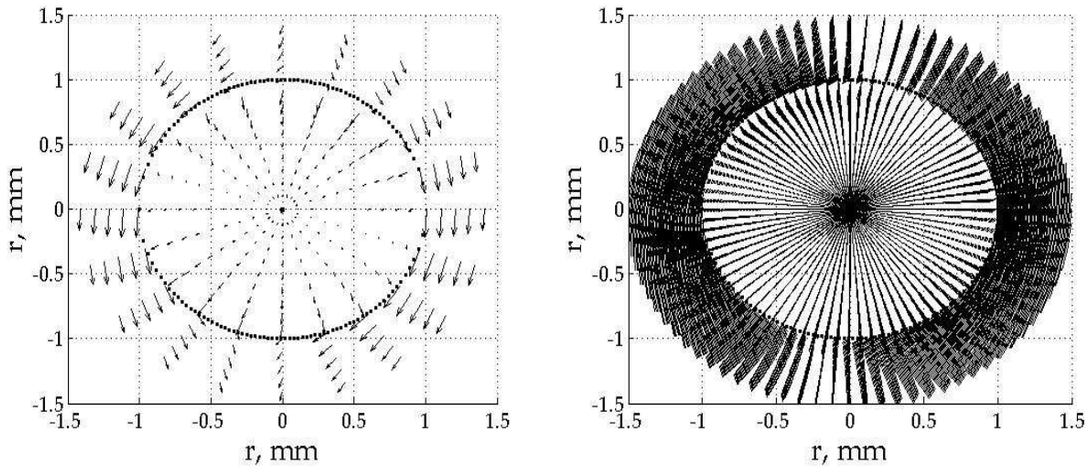

(a) (b)

Fig. 23. The electric field distributions of the main mode at T = 20°C: (a) – the electric field strength lines and (b) – the intensity of the electric field

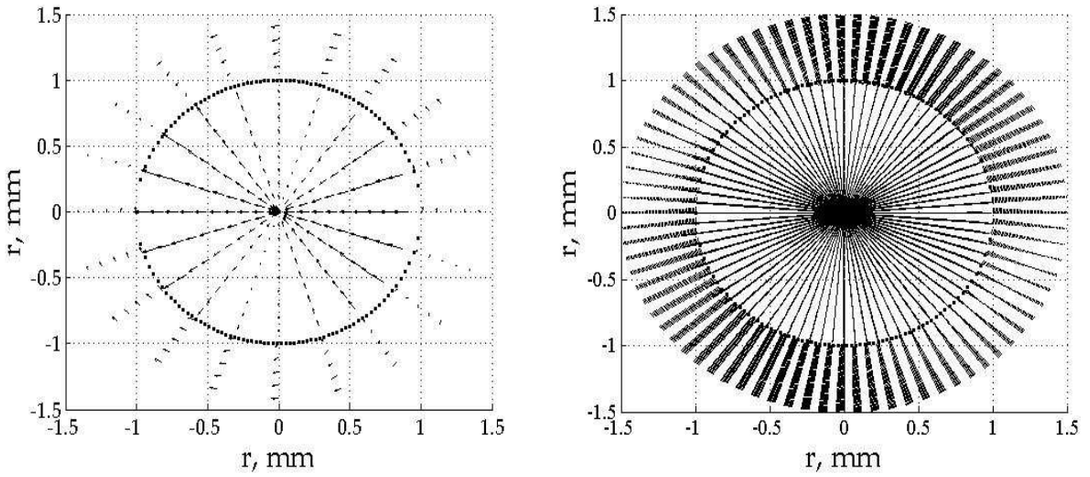

(a) (b)

Fig. 24. The electric field distributions of the main mode at T = 1800°C: (a) – the electric field strength lines and (b) – the intensity of the electric field

The electric field distribution of the main mode (at T = 20°C) presented in Fig. 23 was calculated at f = 103 GHz. The electric field distribution of the main mode (at T = 1800°C) presented in Fig. 24 was calculated at f = 31 GHz. Comparing Fig. 23, 24 we can make a conclusion that the electric fields of the main modes propagating in the hollow-core cylindrical waveguides at T = 20°C and T = 1800°C are different. The strongest electric field of the main mode propagating at T = 20 °C concentrates in the center of hollow-core and closely to the boundary separating SiC and air. However the strongest electric field of the main mode propagating at T = 1800°C concentrates in the air area of the hollow-core waveguide.
The electric field distributions of the first higher modes propagating in the hollow- core SiC waveguide at T = 20°C, shown in Fig. 25, was calculated at f = 135 GHz.

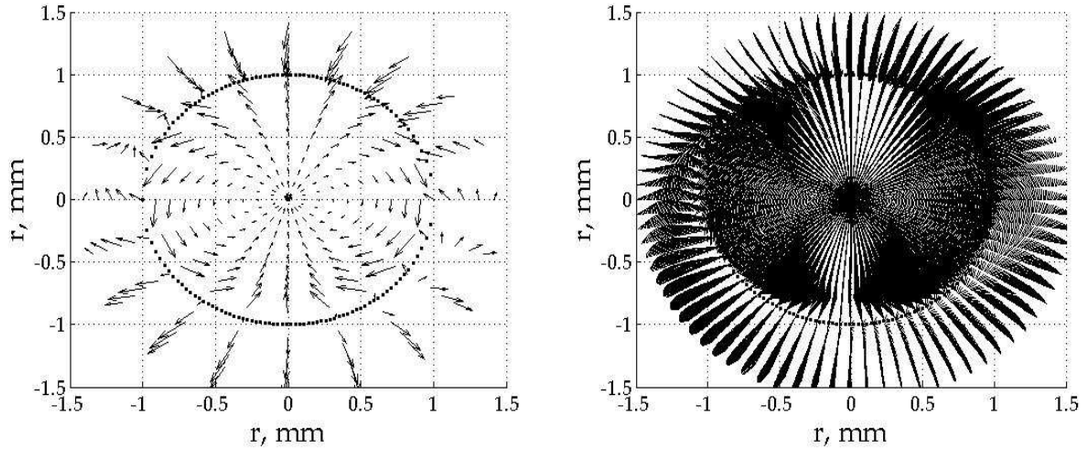

(a) (b)

Fig. 25. The electric field distributions of the first higher mode at T = 20 °C: (a) – the electric field strength lines and (b) – the intensity of the electric field

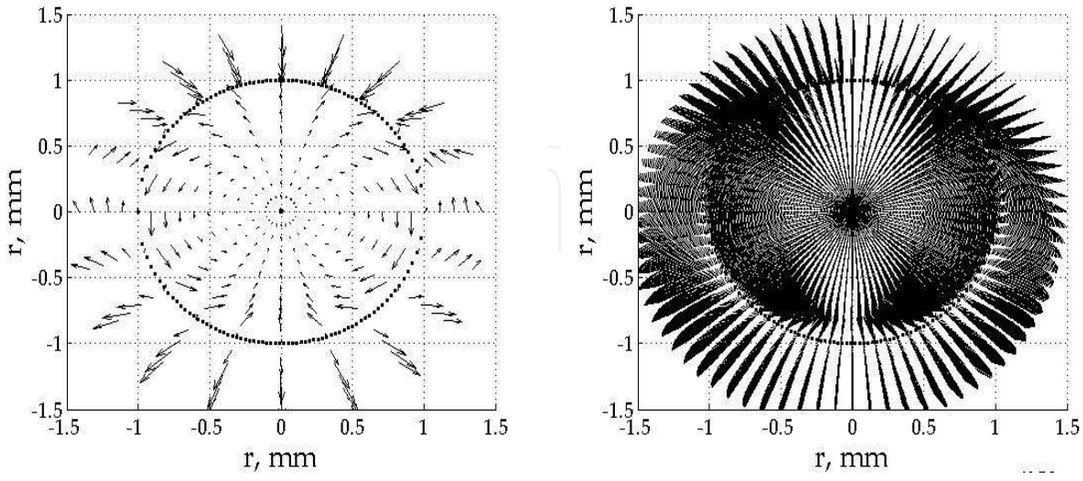

(a) (b)

Fig. 26. The electric field distributions of the first higher mode at T = 1800 °C: (a) – the electric field strength lines and (b) the intensity of the electric field

The electric field distribution of the first higher mode presented at Fig. 26 was calculated at f = 98 GHz. Comparing Figure 25, 26 we can make a conclusion that the electric fields of the first higher modes propagating in the hollow-core cylindrical waveguides at T = 20 °C and T = 1800 °C have similar response.

8. Conclusions

We have fulfilled the electrodynamical analysis of rectangular and circular SiC waveguides. The rectangular waveguides have been investigated by the SIE method, which is very useful and allowed us to analyze waveguides with cross-sections of any intricate shapes. The circular waveguides have been investigated by the partial area method.

Our electrodynamical analysis consists of two steps:

- The calculation of the dispersion characteristics,
- The calculation of the EM field distributions.

The eigenmodes of all investigated SiC waveguides are hybrid modes (Table 1).

We have noted that losses of the main modes propagating in the rectangular waveguides are smaller than losses of the main mode propagating in the circular waveguides at the certain frequencies (compare Figs. 6(b) with 9(b) and Figs. 8 with 13(b)).

We would like to point out that it is possible to find some conditions when the SiC waveguide operates in the single-mode regime and the waveguide broadband width is approximately 25% (Fig. 8).

The losses of the main mode propagating in the circular SiC waveguide have practically invariable values for frequencies ranging from 20-70 GHz. (Fig. 9(b)). This feature is important for operating of modulators and phase shifters which could be created on the basis of such waveguides. The EM signal propagating in the waveguide is not modulated by losses.

Extremely low-loss has a fast wave SiC waveguide. This feature could be used in practice for creation of feeder lines and specific devices that require low losses and low distortions of transmitted signals (Fig. 13(b)).

Thus we can conclude that we have carried out the full electrodynamical analysis of some SiC waveguides. Our investigations can be useful for creation of SiC waveguide devices.

9. References

Agarwal, A. & Ryu, S.-H. (2006). Status of SiC power devices and manufacturing issues, *Proceedings of CS MANTECH Conference*, pp. 215-218, Vancouver, Canada, April 2006

Asmontas S.; Nickelson L.; Bubnelis A.; Martavicius R. & Skudutis J. (2010). Hybrid Mode Dispersion Characteristic Dependencies of Cylindrical Dipolar Glass Waveguides on Temperatures, *Electronics and Electrical Engineering*, Vol. 106, No 10, 83-86, ISSN 1392-1215

Asmontas, S.; Nickelson, L. & Gric, T. (2009). Electric field distributions in the open cylindrical silicon carbide waveguides. *Acta Physica Polonica A,* Vol. 115, No. 6, 1160-1161, ISSN 0587-4254

Asmontas, S.; Nickelson, L. & Plonis D. (2009). Dependences of propagation constants of cylindrical *n*-Si rod on the material specific resistivity, *Electronics and Electrical Engineering*, Vol. 94, No. 6, 57-60, ISSN 1392-1215

Asmontas, S.; Nickelson, L.; Gric, T. & Galwas, B. A. (2009). Solution of Maxwell's equations by the partial area method for the electrodynamical analyses of open lossy metamaterial waveguides, *Proceedings of International Conference Differential Equations and their Applications*, pp. 17-20, ISBN 978-9955-25-747-9, Panevezys, Lithuania, September 2009, KTU, Kaunas, Lithuania

Asmontas, S.; Nickelson, L. & Malisauskas, V. (2006). Investigation of magnetized semiconductor and ferrite waveguides. *Electronics and Electrical Engineering*, Vol. 66, No. 2, 56-61, ISSN 1392-1215

Baeraky, T. A. (2002). Microwave measurements of the dielectric properties of silicon carbide at high temperature. *Egyptian Journal of Solids*, Vol. 25, No. 5, 263–273, ISSN 1012-5566

Bucinskas J.; Nickelson L. & Sugurovas V. (2010). Microwave diffraction characteristic analysis of 2d multilayered uniaxial anisotropic cylinder. *Progress In Electromagnetics Research*, Vol. 109, 175-190, ISSN: 1070-4698

Bucinskas, J.; Nickelson, L. & Sugurovas, V. (2010). Microwave scattering and absorption by a multilayered lossy metamaterial-glass cylinder. *Progress In Electromagnetics Research,* Vol. 105, 103-118, ISSN: 1070-4698

Chen, H.; Wu, B.-I. & Kong A. J. (2006). Review of electromagnetic theory in left-handed materials. *J. of Electromagn. Waves and Appl.*, Vol. 20, No. 15, 2137–2151, ISSN 0920-5071

Gakhov, F.D. (1977). *The boundary problems*, 640 p., Science, Moscow (In Russian)

Gric, T.; Nickelson, L. & Asmontas, S. (2010). Three dimensional magnetic field distributions and dispersion characteristics of rectangular and circular SiC waveguides. *Proceedings of 18th International Conference on Microwaves, Radar and Wireless Communication MIKON-2010*, Vol. 2, pp. 722-725, ISBN 978-9955-690-20-7, Vilnius, June 2010, JUSIDA, Vilnius

Gric T., Nickelson L. & Asmontas S. (2010). 3D vector electric field distributions and dispersion characteristics of open rectangular and circular metamaterial waveguides. *Proceedings of 18th International Conference on Microwaves, Radar and Wireless Communication MIKON-2010*, Vol. 2, pp. 578-581, ISBN 978-9955-690-20-7, Vilnius, Lithuania, June 2010, JUSIDA, Vilnius

Gric T.; Nickelson L., & Asmontas S. (2010). Waveguide Modulator. Patent 5710. Application of Invention 2010-040 is given in *Official bulletin of the state patent bureau of the republic of Lithuania* 2010/11, 2010-11-25, ISSN 1648-9985, Vilnius

Ikeuchi, M.; Sawami, M. & Niki, H. (1981). Analysis of open–type dielectric waveguides by the finite–element iterative method. *IEEE Trans.*, MTT–29, No. 3, 234–239, ISSN 0018-9480

Kajfez, D & Kishk, A. A. (2002). Dielectric resonator antenna − possible candidate for adaptive antenna arrays. *Proceedings of Telecommunications, Next Generation Networks and Beyond International Symposium*, Portoroz, Slovenia, May 2002

Kim, K. Y. (2004). Guided and Leaky Modes of Circular Open Electromagnetic Waveguides: Dielectric, Plasma, and SiC Columns: *Thesis for the Degree of Ph.D.*, 201 p., Kyungpook National University. Daegu, Korea

Kong, J.A. (2008). *Electromagnetic wave theory,* 1016 p., EMW Publishing, ISBN 0-9668143-9-8, Cambridge, Massachusetts, USA

Nickelson L., Galwas B.A., Gric T. & Ašmontas S. (2008). Electric field distributions in the cross sections of the metamaterial hollow-core and rod waveguides, *Proceedings of 17th International Conference on Microwaves, Radar and Wireless Communication MIKON-2008,* Vol. 2, pp. 497-500, ISBN 9781424431229, Wrocław, Poland, May 2008, MDruk, Warszawa, Poland

Nickelson L., Gric T., Asmontas S. & Martavicius R. (2008). Electrodynamical analyses of dielectric and metamaterial hollow-core cylindrical waveguides, *Electronics and Electrical Engineering*, Vol. 82, No 2, 3-8, ISSN 1392-1215

Nickelson L; Gric T; Asmontas S & Martavicius R. (2009) Analyses of the Gyroelectric Plasma Rod Waveguide, *Proceedings of 17th IEEE International Pulsed Power Conference*, (PPC2009) pp. 724-727, Washington

Nickelson L. & Gric, T. (2008). Dispersion characteristics and electric field distributions of modes propagating in the open electrically gyrotropic semiconductor rod waveguide. *Proceedings of 17th International Conference on Microwaves, Radar and Wireless Communication MIKON-2008,* pp. 501-504, ISBN 83-906662-7-8, IEEE Catalog Number: CFPO8784-PRT, Wroclaw, Poland, May 2008, MDruk, Warszawa

Nickelson, L. & Shugurov, V. (2005). *Singular integral equations' method for the analysis of microwave structures*, 348 p., VSP Brill Academic Publishers, ISBN 90-6764-410-2, Leiden-Boston, The Netherlands

Nickelson, L.; Asmontas, S.; Gric, T. & Martavicius, R. (2009). Analysis of Slow and Fast Modes of Lossy Ceramic SiC Waveguides, *Proceedings of Progress In Electromagnetics Research Symposium*, pp. 573-576, ISSN 1159-9450, Moscow, Russia, August 2009, PIERS, Cambridge

Nickelson, L.; Asmontas, S.; Malisauskas, V. & Martavicius, R. (2009). The dependence of open cylindrical magnetoactive p-Ge and p- Si plasma waveguide mode cutoff frequencies on hole concentrations. Journal of Plasma Physics. Vol. 75, 35-51, ISSN 0022-3778

Nickelson, L.; Gric, T.; Asmontas, S. & Martavicius, R. (2009). Electric Field Distributions of the Fast and Slow Modes Propagated in the Open Rod SiC Waveguide. *Electronics and Electrical Engineering*, Vol. 93, No. 5, 87-90, ISSN 1392-1215

Okojie, R. S.; Page, S. M. & Wolff, M. (2006). Performance of MEMS-DCA SiC Pressure Transducers under Various Dynamic Conditions. *Proceedings of IMAPS International High Temperature Electronics Conference*, pp. 70-75, Santa Fe, NM, May 2006

Pandraud, G.; Pham, H. T. M.; French, P. J. & Sarro, P. M. (2007). PECVD SiC optical waveguide loss and mode characteristics. *Optics and Laser Technology*, Vol. 39, No. 3, 532-536

Ponchak, G. E.; Schwartz, Z. D.; Alterovitz, S. A. & Downey, A. N. (2004). Measured Attenuation of Coplanar Waveguide on 6H, p-type SiC and High Purity Semi-Insulating 4H SiC through 800 K. *Proceedings of 12th GAAS Symposium*, pp. 439-442, Amsterdam, the Netherlands, 11-15 October, 2004

IntechOpen

IntechOpen

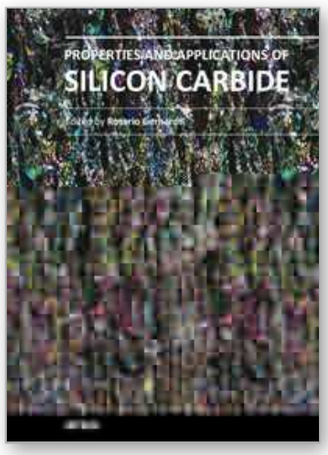

Properties and Applications of Silicon Carbide

Edited by Prof. Rosario Gerhardt

ISBN 978-953-307-201-2
Hard cover, 536 pages
Publisher InTech
Published online 04, April, 2011
Published in print edition April, 2011

In this book, we explore an eclectic mix of articles that highlight some new potential applications of SiC and different ways to achieve specific properties. Some articles describe well-established processing methods, while others highlight phase equilibria or machining methods. A resurgence of interest in the structural arena is evident, while new ways to utilize the interesting electromagnetic properties of SiC continue to increase.

How to reference

In order to correctly reference this scholarly work, feel free to copy and paste the following:

L. Nickelson, S. Asmontas and T. Gric (2011). Electrodynamical Modeling of Open Cylindrical and Rectangular Silicon Carbide Waveguides, Properties and Applications of Silicon Carbide, Prof. Rosario Gerhardt (Ed.), ISBN: 978-953-307-201-2, InTech, Available from: http://www.intechopen.com/books/properties-and-applications-of-silicon-carbide/electrodynamical-modeling-of-open-cylindrical-and-rectangular-silicon-carbide-waveguides

INTECH
open science | open minds

InTech Europe
University Campus STeP Ri
Slavka Krautzeka 83/A
51000 Rijeka, Croatia
Phone: +385 (51) 770 447
Fax: +385 (51) 686 166
www.intechopen.com

InTech China
Unit 405, Office Block, Hotel Equatorial Shanghai
No.65, Yan An Road (West), Shanghai, 200040, China
中国上海市延安西路65号上海国际贵都大饭店办公楼405单元
Phone: +86-21-62489820
Fax: +86-21-62489821

© 2011 The Author(s). Licensee IntechOpen. This chapter is distributed under the terms of the Creative Commons Attribution-NonCommercial-ShareAlike-3.0 License, which permits use, distribution and reproduction for non-commercial purposes, provided the original is properly cited and derivative works building on this content are distributed under the same license.

IntechOpen

IntechOpen